Effect of pressure on segregation in granular shear flows

Alexander M. Fry, Paul B. Umbanhowar, Julio M. Ottino, and Richard M. Lueptow

Phys. Rev. E **97**, 062906 — Published 27 June 2018

DOI: 10.1103/PhysRevE.97.062906

Effect of pressure on segregation in granular shear flows

Alexander M. Fry,[1] Paul B. Umbanhowar,[1] Julio M. Ottino,[1, 2, 3] and Richard M. Lueptow[1, 2, 3]

[1] *Department of Mechanical Engineering, Northwestern University, Evanston, IL 60208, USA*
[2] *Department of Chemical and Biological Engineering, Northwestern University, Evanston, IL 60208, USA*
[3] *The Northwestern Institute on Complex Systems (NICO), Northwestern University, Evanston, IL 60208, USA*

(Dated: May 25, 2018)

The effect of confining pressure (overburden) on segregation of granular material is studied in Discrete Element Method (DEM) simulations of horizontal planar shear flow. To mitigate changes to the shear rate due to the changing overburden, a linear with depth variation in the streamwise velocity component is imposed using a simple feedback scheme. Under these conditions, both the rate of segregation and the ultimate degree of segregation in size bidisperse and density bidisperse granular flows decrease with increasing overburden pressure and scale with the overburden pressure normalized by the lithostatic pressure of the particle bed. At overburdens greater than approximately twenty times the lithostatic pressure at the bottom of the bed, the density segregation rate is zero while the size segregation rate is small but non-zero, suggesting that different physical mechanisms drive the two types of segregation. The segregation rate scales close to linearly with the inertial number for both size bidisperse and density bidisperse mixtures under various flow conditions, leading to a proposed pressure dependence term for existing segregation velocity correlations. Surprisingly, particle stiffness has only a minor effect on segregation, although it significantly affects the packing density.

I. INTRODUCTION

In dense flows of size bidisperse particles, small particles tend to fall into voids between large particles, which forces large particles upward and leads to size segregation in a flowing layer. Likewise, denser particles fall to lower positions, which forces less dense particles upward and leads to density segregation. While most research on segregation in flowing granular mixtures has focused on relatively shallow free surface flows (e.g., heaps, chutes, and tumblers) [1–4], scenarios exist in which granular materials of non-uniform size or density flow under high confining pressures, such as under a translating glacier [5], in an industrial bladed mixer [6], or between bearing surfaces [7–9]. In another example, segregation at the base of size disperse avalanches can lead to increased runout [10, 11]. Hence, the question of how large overburden affects particle segregation is a matter of practical as well as theoretical importance.

Previous experimental research into the connection between overburden pressure and segregation used annular or split bottom shear cells [12, 13] and demonstrated that increasing the overburden decreases the rate of segregation in size bidisperse mixtures of glass spheres. Discrete Element Method (DEM) simulations of horizontal planar shear flow under variable confining pressure have focused on the segregation of low concentrations ($< 10\%$ by volume) of small particles in a bed of large particles [14] or single heavy intruder particles in a bed of light particles [15]. In the former, the rate at which low concentrations of small particles passed through a shearing bed of large particles decreased quickly with the initial increase in overburden pressure, but eventually reached a relatively constant value at higher overburdens [14]. In the single intruder density segregation study, the rate at which single heavy particles sank in a shearing bed of light particles decreased linearly with the square of the overburden pressure over a wide range of normalized overburden pressures, but a relatively narrow range of absolute overburden pressures [15]. However, the effect of confining pressure on segregation in granular materials far from the limit of low concentration of sinking particle species has apparently not been studied systematically.

Here, we use DEM simulations of a confined shear flow to study the effects of overburden pressure on the rate and ultimate degree of segregation in shear flows of equal volume mixtures of size bidisperse or density bidisperse particles. DEM simulations track the dynamics of every particle and allow the overburden to be systematically varied over a wide range of values. Our DEM scheme differs from those used in previous studies on segregation in planar shear flows with variable pressure [14, 15] in two ways. First, we consider equal volume mixtures of particles rather than low concentrations of sinking particles or the single intruder particle limit. Second, we use a proportional control term to enforce a linear velocity profile, whereas the previous studies generated linear velocity profiles by applying gravity to only the sinking particle species. Under these conditions, we find that increasing overburden pressure decreases the rate and ultimate degree of segregation in both size bidisperse and density bidisperse granular shear flows.

The DEM simulations and details of the shear flow are described in Section II. The impact of overburden on segregation of size bidisperse and density bidisperse mixtures is described in Section III. In Section IV, a further series of simulations is presented, in which the shear rate, gravity, mean particle density, and mean par-

ticle diameter are varied to study the impact of the total stress state of the system on segregation and to determine which parameters influence the scaling of the segregation rate and the ultimate degree of segregation with changing overburden. A discussion of the results is provided in Section V.

II. VARIABLE OVERBURDEN SHEAR FLOW

To test the impact of confining pressure (overburden) on segregation in dense granular flows, we employ DEM simulations, which are described in more detail in Appendix A. Millimeter diameter spherical particles are sheared between flat top and bottom frictional planes, with periodic conditions bounding the simulation domain in the streamwise (x) and spanwise (z) directions (see Fig. 1). The massive planar top wall translates horizontally at velocity u_{wall} and is free to move vertically, subject to the force balance between the wall weight and contact forces with the top layer of particles, to enforce a constant average overburden pressure P on the granular bed, with small temporal fluctuations in P as the wall moves up or down to accommodate slight changes in the bed packing. The distance between the upper and lower plates is h, which remains relatively constant (within 1%) after the initial rapid dilation of the particles at the onset of flow. The simulation domain is $l = 280\,\text{mm}$ in the streamwise direction, $w = 35\,\text{mm}$ in the spanwise direction, and $h \approx 25\,\text{mm}$ in the vertical direction. Segregation results at identical pressure and flow conditions in a domain with double the spanwise periodic width ($w = 70\,\text{mm}$) are indistinguishable from the results of the simulations presented here (with $w = 35\,\text{mm}$), confirming that the periodic domain is large enough to have no impact on the results. In most cases the gravitational acceleration is $g = 9.8\,\text{m/s}^2$, though a few simulations in Section IV have a higher gravitational acceleration to explore a broader range of conditions and to validate the pressure scaling.

Most size bidisperse simulations were performed for a large to small particle diameter ratio $d_L/d_S = 2$ ($d_S = 2\,\text{mm}$ and mean diameter $d_L = 4\,\text{mm}$ particles; $\bar{d} = 3\,\text{mm}$) and particle density $\rho = 2500\,\text{kg/m}^3$, and most density bidisperse simulations were performed for a high to low density ratio $\rho_H/\rho_L = 9$ ($\rho_H = 4500\,\text{kg/m}^3$ and $\rho_H = 500\,\text{kg/m}^3$; $\bar{\rho} = 2500\,\text{kg/m}^3$) and particle diameter $d = 3\,\text{mm}$. The number of particles in a simulation ranged from 10000 to 100000. Particle species of a given nominal size have a uniformly distributed size polydispersity of $\pm 10\%$ in size bidisperse cases and $\pm 20\%$ in density bidisperse cases to avoid particle layering or other ordering. For the limited number of simulations carried out for other particle sizes in Section IV, the same distance ($h \approx 25\,\text{mm}$) was maintained between the plates. The size ratio was chosen to be below the free sifting regime but large enough to result in significant segregation, and the density ratio was chosen so that the segregation velocity – the characteristic velocity at which small or heavy particles sink in the flow and large or light particles rise in the flow – is similar to that for the size case at low overburden (free surface flows) as determined from previous studies of size [16] and density [17] segregation. Since the segregation behaviors are similar for these size and density ratios for free surface conditions, it is possible to compare the effects of increasing overburden between size and density segregation. The binary collision time was also varied over the range $1.25 \times 10^{-4}\,\text{s} \leq t_c \leq 1 \times 10^{-3}\,\text{s}$, which results in a range of particle stiffnesses $63\,\text{N/m} \leq k_n \leq 5909\,\text{N/m}$, to determine the effect of particle deformation on segregation.

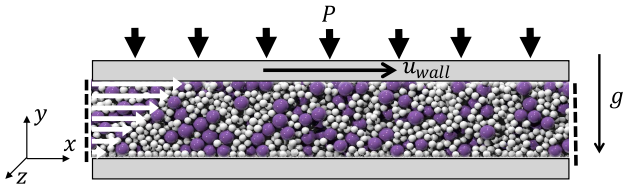

FIG. 1. Schematic (side view) of size bidisperse shear flow 0.5 s after the onset of shear but before significant segregation has occurred. Vertical dashed lines represent streamwise periodic boundary conditions; the domain is also periodic in the spanwise direction. The top and bottom walls are modeled as flat frictional planes. Top wall mass is varied to change the overburden pressure P, and the top wall is free to move vertically due to dilation or compaction of the bed particles. Particle sizes are $d_S = 2\,\text{mm}$ and $d_L = 4\,\text{mm}$ in the simulation shown. The particle bed shown here is truncated in the streamwise direction compared to actual simulations.

The shear rate, which directly affects segregation [2, 16–18], was controlled to be constant through the depth in each simulation, rather than allowing it to develop naturally, because the overburden affects the velocity profile, altering both its shape and fluctuations about the mean profile. Keeping the shear rate fixed allows the intrinsic effects of the overburden on segregation to be studied without the complication of a spatially varying velocity gradient. A linear velocity profile is maintained by applying a stabilizing force in the streamwise direction on each particle at every timestep according to

$$F_{stabilize} = A(\dot{\gamma} y - u_x), \tag{1}$$

where u_x is the particle's streamwise velocity, y is the particle's vertical position, $\dot{\gamma}$ is the imposed global shear rate, and A is a control parameter. A similar stabilizing force scheme has been used to control the velocity profile in simulations of hard frictionless particles [19], though the particles here are deformable and frictional. Since the normal and frictional forces that tend to destabilize the velocity profile scale with the local pressure, A is varied proportionally to the local pressure in the bed [20]. Thus, the streamwise velocity profiles in these simulations are the result of the combination of the motion of

the upper and lower walls and the stabilizing forces. The top wall translates at a streamwise velocity $u_{wall} = \dot{\gamma}h$ determined by the imposed shear rate and the wall's vertical location, which is free to adjust to the dilation or compaction of the particle bed.

The streamwise velocity profile for a size bidisperse simulation, 0.5 seconds after flow is initiated, is shown in Fig. 2. At this time the flow is steady, but little segregation has occurred. It is clear that the mean velocity profile is linear so that the shear rate is uniform through the depth of the particle bed. The velocity fluctuations are relatively uniform about the mean profile, except for the regions adjacent to each wall, where the fluctuations are somewhat larger due to collisions with randomly located particles in the bulk and with the flat frictional wall. Distinct layers of particles are noticeable at $\sim d_S/2$ and $\sim d_L/2$ away from both walls, due to particle ordering adjacent to the flat walls. Since these artifacts of the geometry in the velocity profile are common to all of the simulations at varying flow conditions, they are unlikely to affect the trends in this study.

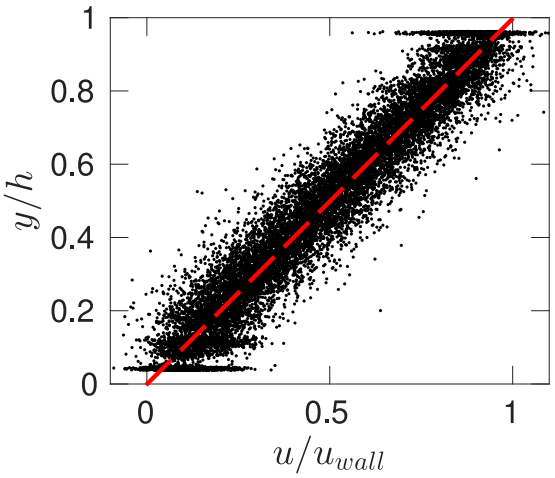

FIG. 2. Streamwise velocities of individual particles in a size bidisperse simulation with species diameter ratio $d_L/d_S = 2$, shear rate $\dot{\gamma} = 5\,\mathrm{s}^{-1}$, and overburden pressure $P = 340\,\mathrm{Pa}$. Particle sizes are $d_S = 2\,\mathrm{mm}$ and $d_L = 4\,\mathrm{mm}$. Data are recorded for all particles in the simulation at an instant 0.5 seconds after onset of shear, at which point the particles are still relatively well-mixed.

III. INFLUENCE OF OVERBURDEN ON SEGREGATION

The impact of the overburden on segregation is shown in Fig. 3 for equal volume mixtures of size bidisperse particles with size ratio $d_L/d_S = 2$, $d_L = 4\,\mathrm{mm}$, and $d_S = 2\,\mathrm{mm}$ (left column) and density bidisperse particles with density ratio $\rho_H/\rho_L = 9$ and $d = 3\,\mathrm{mm}$ (right column). The steady-state segregation after 100 s of simulation is shown for a shear rate of $\dot{\gamma} = 5\,\mathrm{s}^{-1}$ for three different overburden pressures. It is clear that the steady state segregation decreases as overburden increases. Almost complete segregation occurs for a smaller overburden of $P = 85\,\mathrm{Pa}$, while very little segregation occurs for a larger overburden of $P = 1358\,\mathrm{Pa}$. Since the streamwise velocity profile is the same for all cases, the changes in segregation are only due to changes in the overburden.

A. Quantifying segregation

To characterize the evolution of the segregation at various overburden pressures, we measure the average center of mass height of the rising (large or less dense) particle species, $\bar{y}_R$, relative to the mean height of all the particles in the bed, $\bar{y}$, such that $y_R = \bar{y}_R - \bar{y}$, noting that $\bar{y} \approx h/2$. For a perfect mixture, $y_R = 0$. A time series of y_R is plotted for a size bidisperse mixture in Fig. 4 at $P = 340\,\mathrm{Pa}$. Similar time evolution of the rising particle species height occurs for density bidisperse mixtures (not shown). The particles start from an initially mixed state, segregate over time, and eventually saturate at a state somewhere between perfectly mixed and perfectly segregated. This behavior has been shown previously in experiments on confined granular shear flows at relatively low overburden pressures [12, 13], and can be understood in terms of a segregation-diffusion balance [18, 21–24], typically expressed in terms of an advection-diffusion equation for each particle species with an added segregation term. That is, at steady-state the magnitude of the directed rearrangement mechanism of segregation balances the random collisional diffusion mechanism that remixes particles. Furthermore, when the system becomes highly segregated, large or light particles can sometimes become trapped in regions with many small or heavy particles, which limits the ultimate degree of segregation [13, 25–28].

Two key characteristics of the system can be determined from the evolution of the segregation shown in Fig. 4. First, the final height of the rising species $y_{R,f}$ is calculated as the mean center of mass height over the last 10 seconds of the simulation. Second, the rate of segregation w_S during the rapidly segregating transient at the start of the simulation is calculated as $y_{R,f}/(2\tau)$ where τ is the time for the system to segregate to one-half of its final value. Similar trends for segregation rate are found using sampling windows defined in other ways, as long as the sampling window falls within the rapidly segregating timescale. This rate of segregation w_S is closely related to the percolation velocity $w_{p,i}$ discussed in previous studies [15–18], since it is essentially the average rate at which species rise or fall relative to the mean flow. The segregation rates w_S at the lowest overburden conditions in this paper are about 15% less than the percolation velocities predicted by previous studies of size bidisperse [16] and density bidisperse [17] segregation of mm-sized particles in free surface flows, which is not surprising since the

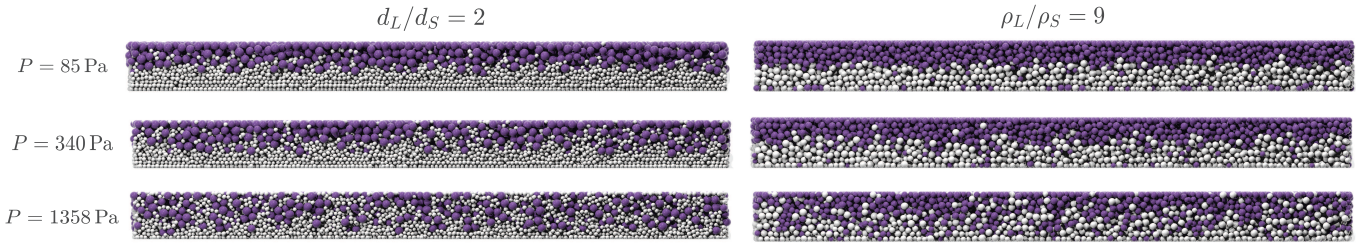

FIG. 3. Sideview images of simulation domain at steady state after 100 s of shear flow in $d_L/d_s = 2$ size bidisperse (left) and $\rho_H/\rho_L = 9$ density bidisperse (right) mixtures. For both types of mixtures, the steady state degree of segregation decreases with increasing overburden pressure. Particle sizes are $d_S = 2\,\mathrm{mm}$ and $d_L = 4\,\mathrm{mm}$ for size bidisperse mixtures with particle density $\rho = 2500\,\mathrm{kg/m^3}$, and $d = 3\,\mathrm{mm}$ for density bidisperse mixtures with particle densities $\rho_H = 4500\,\mathrm{kg/m^3}$ and $\rho_L = 500\,\mathrm{kg/m^3}$. The binary collision time is $t_c = 1.25 \times 10^{-4}\,\mathrm{s}$, corresponding to particle normal stiffness $k_n = 5909\,\mathrm{N/m}$ for the size bidisperse mixtures and $k_n = 4039\,\mathrm{N/m}$ for the density bidisperse mixtures.

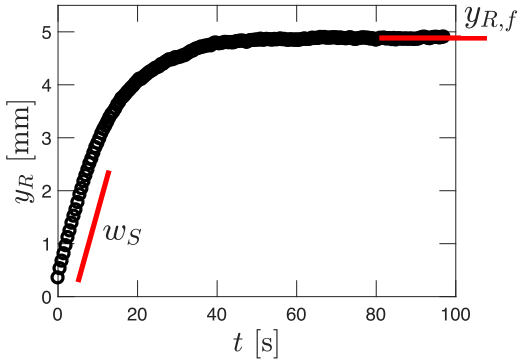

FIG. 4. Time series of the rising particle species center of mass y_R for a size bidisperse mixture ($d_L/d_S = 2$) with binary collision time $t_c = 1.25\times10^{-4}\,\mathrm{s}$ (particle stiffness $k_n = 5909\,\mathrm{N/m}$), overburden pressure $P = 340\,\mathrm{Pa}$, and shear rate $\dot\gamma = 5\,\mathrm{s}^{-1}$. w_S characterizes the initial rate of segregation, and $y_{R,f}$ measures the final height of the rising particle species. Particle diameters are $d_S = 2\,\mathrm{mm}$ and $d_L = 4\,\mathrm{mm}$, and particle density is $\rho = 2500\,\mathrm{kg/m^3}$.

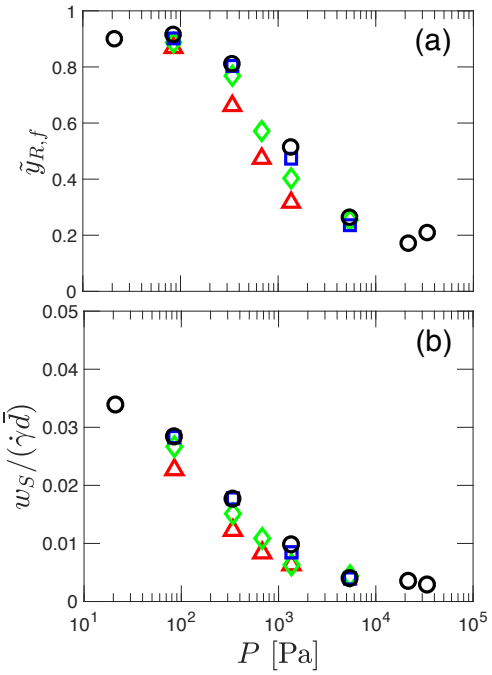

FIG. 5. (a) Normalized final height of large particle species $\tilde y_{R,f}$ and (b) normalized segregation rate $w_S/(\dot\gamma\bar d)$ vs. overburden P for size ratio $d_L/d_S = 2$, $d_S = 2\,\mathrm{mm}$, $d_L = 4\,\mathrm{mm}$, and shear rate $\dot\gamma = 5\,\mathrm{s}^{-1}$. $t_c = 1 \times 10^{-3}\,\mathrm{s}$, $k_N = 92\,\mathrm{N/m}$ (△); $t_c = 5 \times 10^{-4}\,\mathrm{s}$, $k_N = 370\,\mathrm{N/m}$ (◇); $t_c = 2.5 \times 10^{-4}\,\mathrm{s}$, $k_N = 1477\,\mathrm{N/m}$ (□); $t_c = 1.25 \times 10^{-4}\,\mathrm{s}$, $k_N = 5909\,\mathrm{N/m}$ (○).

flows here are bounded above by a top wall that still has a finite mass even at the lowest overburden conditions.

Note that the mixed state in Fig. 4 at the onset of shear deviates slightly from a perfectly mixed system (i.e. $y_R = 0$) because some segregation occurs during the initialization process. To build the system, particles are created in a grid pattern and settle under the force of gravity, during which time some segregation occurs. Since this segregation is unrelated to the shear flow being studied, w_S is calculated from the initial point ($y_{R,0} \neq 0$ at $t = 0$) instead of from a perfectly mixed state.

To quantify the impact of overburden on segregation, the normalized final center of mass height $\tilde y_{R,f} = y_{R,f}/(h/4)$ and the normalized rate of segregation $w_S/(\dot\gamma d)$ are plotted versus the overburden pressure for size (Fig. 5) and density (Fig. 6) bidisperse simulations. For perfectly mixed particles, the center of mass of the rising particles is $\bar y_R = h/2$ so that $y_R = h/2 - h/2 = 0$, while for perfectly segregated particles, the rising particles fill the upper half of the domain so that $\bar y_R = 3h/4$ and $y_R = 3h/4 - h/2 = h/4$. Thus, when the the center of mass height is normalized by $h/4$, it lies between 0 (perfectly mixed) and 1 (perfectly segregated). The rate of segregation is non-dimensionalized by the characteristic velocity in the shearing granular flow $\dot\gamma\bar d$, consistent with previous studies of the percolation velocity [16–18]. In Figs. 5 and 6, the different symbols represent results for simulations of particles with different particle stiffness. The ultimate degree of segregation and the rate of segregation decrease with increasing overburden and are only weakly dependent on particle stiffness

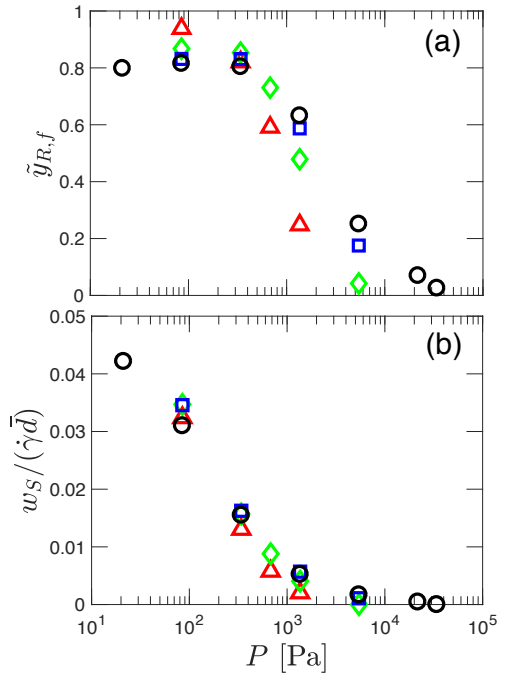

FIG. 6. (a) Normalized final height of less dense particle species $\tilde{y}_{R,f}$ and (b) normalized segregation rate $w_S/(\dot{\gamma}\bar{d})$ vs. overburden P for density ratio $\rho_H/\rho_L = 9$, $d = 3\,\mathrm{mm}$, and shear rate $\dot{\gamma} = 5\,\mathrm{s}^{-1}$. $t_c = 1 \times 10^{-3}\,\mathrm{s}$, $k_N = 63\,\mathrm{N/m}$ (△); $t_c = 5 \times 10^{-4}\,\mathrm{s}$, $k_N = 252\,\mathrm{N/m}$ (◇); $t_c = 2.5 \times 10^{-4}\,\mathrm{s}$, $k_N = 1010\,\mathrm{N/m}$ (□); $t_c = 1.25 \times 10^{-4}\,\mathrm{s}$, $k_N = 4039\,\mathrm{N/m}$ (○).

even when particle deformation (equivalent to overlap in DEM simulations) becomes large. At low overburden, $\tilde{y}_{R,f} \approx 0.9$ for both size and density bidisperse mixtures, while $w_S/(\dot{\gamma}\bar{d}) \approx 0.035$ for size bidisperse mixtures and $w_S/(\dot{\gamma}\bar{d}) \approx 0.04$ for density bidisperse mixtures. As the overburden increases, $\tilde{y}_{R,f}$ and $w_S/(\dot{\gamma}\bar{d})$ decrease for both size and density bidisperse mixtures, indicating reduced segregation. At the highest overburdens tested, $\tilde{y}_{R,f}$ and $w_S/(\dot{\gamma}\bar{d})$ go nearly to zero for density segregation, while they remain at small non-zero values for size segregation.

B. Packing fraction

In many models of size segregation, segregation is assumed to occur when small particles percolate downward through voids, while large particles are squeezed upward [2, 18, 29]. A somewhat different scenario has been proposed to explain density segregation in which less dense particles require smaller forces to support them than more dense particles, leading to a propensity for less dense particles to be forced upward in the flow more easily than more dense particles [17, 30, 31]. In both cases, the generation of voids as the material flows is assumed to be crucial to segregation. To ensure that the overburden is not simply reducing segregation by causing the deformable particles to overlap to a point at which they cannot rearrange, we consider the relation between final segregation state and packing fraction to determine if it explains the observed decrease in segregation with increasing overburden in terms of the availability of voids through which particles can percolate.

The packing fraction, ϕ, is plotted as a function of overburden for simulations with various particle stiffnesses in Fig. 7(a) for cases of size segregation and in Fig. 8(a) for cases of density segregation. The packing fraction is calculated as the ratio of particle volume to total volume in the middle 1/3 of the particle bed ($y/h = 1/3$ to $y/h = 2/3$) 0.5 s after the initiation of shear, when the flow is steady but the particle bed is still well-mixed. After the initial dilation due to the onset of shear, ϕ decreases by less than 1% over the course of the entire simulation for all simulations. The packing fraction is a function of both overburden pressure and particle stiffness, with particles packing more closely under both higher overburden pressure and at lower particle stiffness. The packing fraction data can be collapsed by plotting it against the effective particle stiffness – the dimensionless ratio between particle stiffness and overburden, $\kappa = k_n/(P\bar{d})$. This effective particle stiffness is proportional to the deflection at particle contacts normalized by particle diameter as a result of typical normal forces in the system [32]. As evident in Figs. 7(b) and 8(b), ϕ in a steady-flowing mixed state is well characterized by $1/\kappa$ across a range of absolute stiffnesses and overburdens. The packing fraction is large at high pressures and low effective particle stiffness (small κ) when the particles undergo significant deformation. The packing fraction decreases and then plateaus at high effective particle stiffness when particles deform less (large κ). Size bidisperse mixtures asymptote to a slightly tighter packing than density bidisperse mixtures, because particles of different sizes pack more efficiently than particles of a single size (as in the density bidisperse cases) as small particles fill gaps between large particles [33].

To examine the relation between packing fraction and segregation, the normalized final height of the rising particle species, $\tilde{y}_{R,f}$, is plotted as a function of ϕ for various overburden pressures and particle stiffnesses in Fig. 9. While segregation decreases with increasing packing fraction for any individual particle stiffness, it decreases more quickly for stiffer particles than for softer particles. If segregation were purely dependent on voids through which particles percolate, segregation should change similarly at different particle stiffnesses simply as a function of void density, measured here in terms of packing fraction. Since this is not the case, and since segregation is clearly a function of changing overburden pressure (see Figs. 5 and 6), segregation in these dense shear flows is not purely a function of void spacing. Figure 9 also shows that segregation can be similar for DEM particles with low and high effective particle stiffnesses, even though soft particles are packed to higher packing fractions than stiff particles.

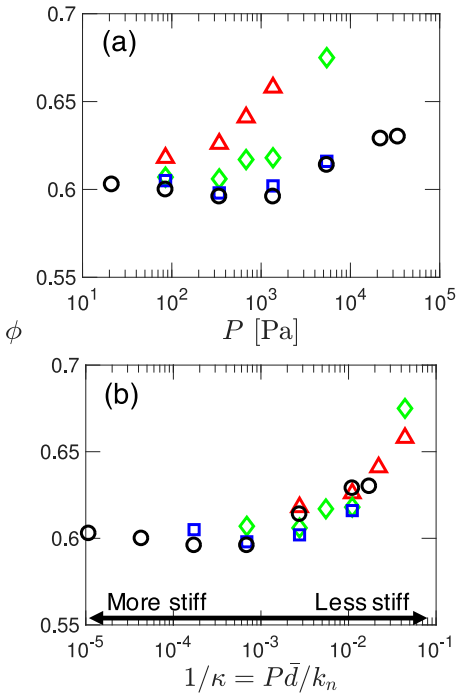

FIG. 7. Mean packing fraction ϕ vs. (a) overburden P and (b) the inverse of effective particle stiffness $1/\kappa = P\bar{d}/k_n$ for size bidisperse simulations. Symbols as in Fig. 5.

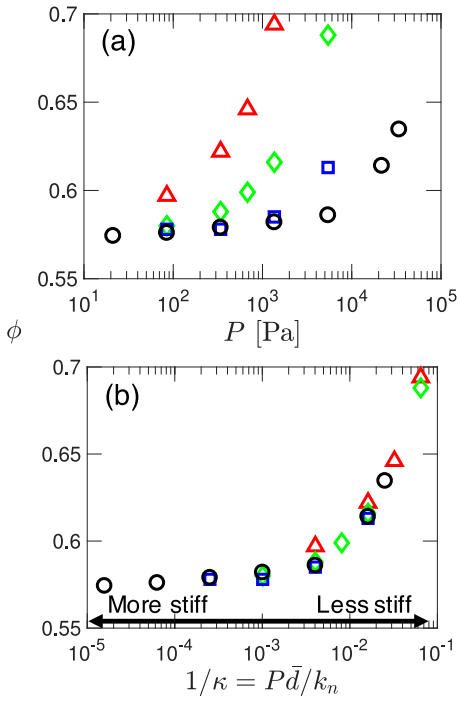

FIG. 8. Mean packing fraction ϕ vs. (a) overburden P and (b) the inverse of effective particle stiffness $1/\kappa = P\bar{d}/k_n$ for density bidisperse simulations. Symbols as in Fig. 6.

IV. SEGREGATION SCALING WITH OVERBURDEN

To understand the effect of the overburden pressure on segregation within the broader context of the full stress state in granular shear flow, it is helpful to consider not only the normal stress changes but also the changes in shear stress. To test the effect of the combined normal and shear stress conditions on segregation in both size bidisperse and density bidisperse shear flows, we performed additional simulations (see Table I) for a broader range of conditions: shear rates $\dot{\gamma} = 2.5\,\mathrm{s}^{-1}$, $\dot{\gamma} = 10\,\mathrm{s}^{-1}$, and $\dot{\gamma} = 25\,\mathrm{s}^{-1}$, gravitational acceleration $g = 19.6\,\mathrm{m/s}^2$, mean particle densities $\bar{\rho} = 1250\,\mathrm{kg/m}^3$ and $\bar{\rho} = 5000\,\mathrm{kg/m}^3$, and mean particle diameter $\bar{d} = 1.5\,\mathrm{mm}$ ($d_S = 1\,\mathrm{mm}$ and $d_L = 2\,\mathrm{mm}$ for size bidisperse and $d = 1.5\,\mathrm{mm}$ for density bidisperse). All of these simulations use particles with binary collision time $t_c = 1.25\times10^{-4}\,\mathrm{s}$, which corresponds to the stiffest particles considered in Section III. Although particle stiffness varies with effective mass (see Appendix A) so that it depends on absolute particle size and density in addition to binary collision time, the changes in segregation due to the effective mass dependence of particle stiffness are minimal compared to the effect of overburden and flow conditions for this series of simulations.

TABLE I. Simulation conditions for data in Figs. 10 – 12

Symbol	$\bar{d}$ [mm]	$\bar{\rho}$ [kg/m^3]	$\dot{\gamma}$ [s^{-1}]	g [m/s^2]
▼	3	2500	2.5	9.8
○	3	2500	5	9.8
▶	3	2500	10	9.8
▲	3	2500	25	9.8
★	3	2500	5	19.6
♦	3	1250	5	9.8
■	3	5000	5	9.8
●	1.5	5000	5	9.8

A. Scaling with lithostatic pressure

The normalized final mean rising particle height $\tilde{y}_{R,f}$ for size and density bidisperse cases is plotted in Fig. 10 as a function of overburden pressure normalized by the lithostatic pressure of the particle bed, $P/(\rho_B g h)$, where ρ_B is the bulk density in the bed. The lithostatic pressure remains constant during each simulation and is equivalent to the weight of the bed of particles divided by the area of the bottom of the shear cell, i.e. $\rho_B g h = m_B g/(lw)$. Considering first size segregation in Fig. 10(a), data for the normalized final height $\tilde{y}_{R,f}$ at various overburden pressures, shear rates, gravitational accelerations, mean particle diameters, and mean particle densities collapse onto a single curve when plotted

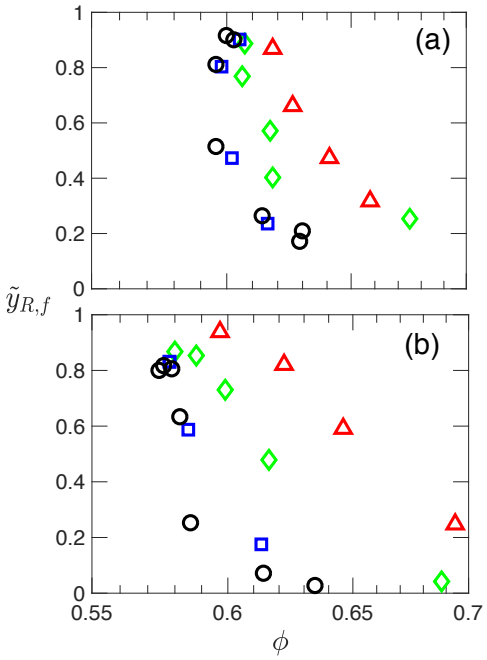

FIG. 9. Normalized final height of large particle species $\widetilde{y}_{R,f}$ vs. mean packing fraction ϕ for (a) $d_L/d_S = 2$ size bidisperse simulations and (b) $\rho_H/\rho_L = 9$ density bidisperse simulations. Symbols as in Fig. 5 (size bidisperse data) and Fig. 6 (density bidisperse data).

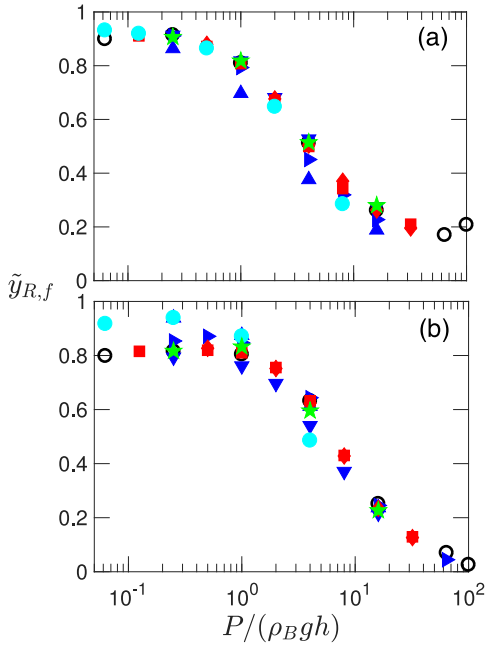

FIG. 10. Normalized final height of large particle species $\widetilde{y}_{R,f}$ vs. normalized overburden pressure $P/(\rho_B g h)$ for (a) $d_L/d_S = 2$ size bidisperse simulations and (b) $\rho_H/\rho_L = 9$ density bidisperse simulations for the conditions described in Table I; $t_c = 1.25 \times 10^{-4}$ s.

versus $P/(\rho_B g h)$. The collapse of the data indicates that the ultimate degree of segregation is insensitive to shear rate. This is not unexpected, because the competing effects of segregation ($w_{p,i} \sim \dot{\gamma} d$ [16–18]) and diffusion ($D \sim \dot{\gamma} d^2$ [34–36]) are both proportional to the shear rate resulting in a steady state that is independent of shear rate [37]. Additionally, we measured the diffusion and confirmed that it is essentially independent of pressure, P (as well as mean particle density, $\bar{\rho}$, and gravity, g, for the cases tested), but is a function of $\dot{\gamma} d^2$, consistent with previous research [34–36]. Since segregation decreases with increasing pressure, while diffusive remixing is independent of pressure, the steady-state degree of segregation in the system decreases with increasing pressure. Much like in the size bidisperse cases, the normalized final height data for density bidisperse simulations in Fig. 10(b) also collapse reasonably well when plotted versus $P/(\rho_B g h)$, except for some small deviations at low normalized overburden ($P/(\rho_B g h) \leq 1$). Again, shear rate has no effect on the ultimate degree of segregation.

Figure 10 shows that density segregation ceases at a critical overburden pressure, while size segregation occurs to a small degree at large overburdens. This suggests differences in the underlying segregation mechanism for size segregation compared to density segregation. The cessation of density segregation was not observed in a previous study of single intruder particle density segregation, perhaps because the maximum overburden pressure ($P \leq 156$ Pa [15]) was much smaller than in this study ($P \leq 34$ kPa).

The non-dimensional rate of segregation $w_S/(\dot{\gamma}\bar{d})$ for the size bidisperse and density bidisperse simulations is plotted as a function of $P/(\rho_B g h)$ in Fig. 11. In both cases, the non-dimensional segregation rate at varying overburden pressure collapses for some of the varying conditions ($\dot{\gamma}$, g, and $\bar{\rho}$) but less well for cases with varying mean particle size $\bar{d}$ (an alternative scaling is discussed in Section IV B). The segregation rate behavior at the extremes of overburden can be seen more clearly in Fig. 11 (insets), in which the segregation rate data are instead plotted on log-log axes. At low overburdens segregation rate appears to be approaching a finite value with decreasing $P/(\rho_B g h)$ for both size bidisperse and density bidisperse mixtures. Note that the lithostatic pressure beneath a single layer of particles corresponds to $\rho_B g \bar{d} = \rho_B g h/8$, for $\bar{d} = 3$ mm particles, or $\rho_B g \bar{d} = \rho_B g h/16$, for $\bar{d} = 1.5$ mm particles. Similar to the trends for the normalized final height data, at high overburdens the segregation rate data for size disperse mixtures have small finite values as $P/(\rho g h)$ increases, while the segregation rate data for density bidisperse mixtures go effectively to zero above a critical pressure. The appearance of an asymptote in the rate of segregation at high normalized overburden pressure was previously observed for size segregation of a low concentration of small particles [14].

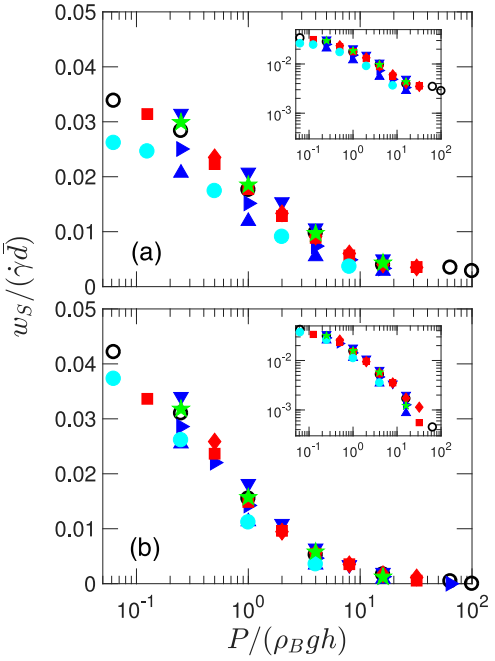

FIG. 11. Normalized segregation rate $w_S/(\dot{\gamma}\bar{d})$ vs. normalized overburden pressure $P/(\rho_B g h)$ for (a) $d_L/d_S = 2$ size bidisperse simulations and (b) $\rho_H/\rho_L = 9$ density bidisperse simulations for the conditions described in Table I; $t_c = 1.25 \times 10^{-4}$ s. The same data are plotted on log-log axes in the insets.

B. Scaling with inertial number

Some features of the segregation rate scaling with overburden are quite apparent in Fig. 11 – the collapse of data at varying system conditions, the cessation of density segregation rate above a critical overburden, and only a small degree of size segregation at high overburdens. However, the functional form of the segregation scaling with overburden is unclear. Furthermore, while the lithostatic pressure $\rho_B g h$ appears to be a useful way to non-dimensionalize the pressure for the normalized rising species final height $\widetilde{y}_{R,f}$ data, it is less satisfactory in collapsing the segregation rate $w_S/(\dot{\gamma}d)$ data. Ideally, a non-dimensionalization approach would collapse the data onto a single curve with a functional form based on the physics of the situation. In search of this functional form and to connect segregation to other work in granular flow modeling, we examine the data in terms of the inertial number $I = \dot{\gamma}\bar{d}/\sqrt{P/\bar{\rho}}$ [38], which is a non-dimensional quantity that captures the pressure-shear stress state in granular flow. The inertial number is normally calculated using local values of $\dot{\gamma}$, $\bar{d}$, $\bar{\rho}$, and P, but since the segregation rate is an average value across the entire shear cell, a single global inertial number is calculated here for each simulation using the overburden P and the average values of $\dot{\gamma}$, $\bar{d}$, and $\bar{\rho}$.

Previous research has shown that certain granular flow characteristics are reliably dependent on the inertial number, including velocity profiles, the flowing layer depth, and the volume fraction in various geometries (planar shear, annular shear, chutes, and heaps) [38, 39]. A recent study on the connection between granular flow rheology and density segregation demonstrated that segregation rates of a single heavy intruder particle in a planar shear flow of light particles collapse onto a single curve for simulations under various pressure and flow conditions when plotted as a function of the inertial number [15]. Since our simulations are far from the low sinking particle concentration limit, examine both size and density segregation, and explore a much wider range of overburden pressures, they provide an ideal opportunity to determine if the segregation rate depends on the inertial number more generally for segregating granular shear flows.

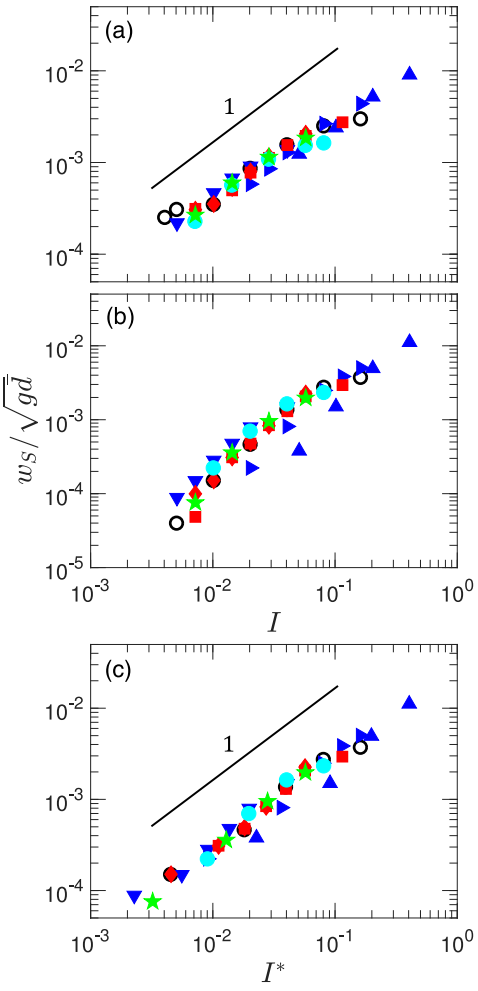

FIG. 12. Normalized segregation rate $w_S/\sqrt{g\bar{d}}$ vs. inertial number $I = \dot{\gamma}\bar{d}/\sqrt{P/\bar{\rho}}$ for (a) $d_L/d_S = 2$ size bidisperse simulations and (b) $\rho_H/\rho_L = 9$ density bidisperse simulations for the conditions described in Table I; $t_c = 1.25 \times 10^{-4}$ s. (c) The same normalized segregation rate $w_S/\sqrt{g\bar{d}}$ data for density bidisperse simulations vs. inertial number accounting for a critical pressure cutoff $I^* = \dot{\gamma}\bar{d}/\sqrt{[P/(1-P/P_{crit})]/\bar{\rho}}$, where $P_{crit} = 20\rho g h$.

To test this, $w_S/\sqrt{g\bar{d}}$ is plotted as a function of inertial number I in Figs. 12(a) and 12(b), for size bidisperse and density bidisperse data, respectively [40]. For size segregation, the data collapse for all cases (varying P, $\dot{\gamma}$, g, $\bar{\rho}$, and $\bar{d}$) onto a single curve as a function of inertial number. Although the dependence of $w_S/\sqrt{g\bar{d}}$ on I is not linear (a slope of 0.84 rather than 1), the collapse is excellent. However, applying the same approach to the density bidisperse data does not collapse the data as a function of inertial number [Fig. 12(b)]. This is because density segregation ceases at large values of normalized overburden, evident in Fig. 11(b). To account for the cessation of density segregation at a finite value of overburden, we instead plot $w_S/\sqrt{g\bar{d}}$ in Fig. 12(c) versus the inertial number accounting for a critical pressure cutoff $I^* = \dot{\gamma}\bar{d}/\sqrt{[P/(1-P/P_{crit})]/\bar{\rho}}$. Here, P_{crit} is the critical pressure at which density segregation effectively ceases. A value of $P_{crit} = 20\rho gh$ collapses the segregation rate data for all of the flow conditions onto a single curve, though data for the highest shear rate ($\dot{\gamma} = 25\,\mathrm{s}^{-1}$) tend to be on the low side of the curve. The dependence of $w_S/\sqrt{g\bar{d}}$ on I is closer to linear (a slope of 0.94) for the the density bidisperse data in Fig. 12(c) than for the size bidisperse data in Fig. 12(a). Note that the critical pressure here is specific to $\rho_H/\rho_L = 9$. In general, it may be a function of the density ratio. It is important to further note that the data in Figs. 12(a,c) closely overlay one another if superimposed, indicating similar dependence of segregation rate on inertial number for both size and density segregation (when the critical pressure is accounted for).

We now consider the relation between the inertial number I and the percolation velocity $w_{p,i}$ described in previous studies [16–18] and shown to be consistent with the kinetic sieving/squeeze expulsion theory of Savage and Lun [2] for free surface flows in which the effect of the lithostatic pressure is negligible [27]. For free surface flows, the percolation velocities for species i for size and density segregation are, respectively:

$$w_{p,i} = S_S\dot{\gamma}(1-c_i), \tag{2}$$

$$w_{p,i} = S_D\dot{\gamma}(1-c_i), \tag{3}$$

where c_i is the concentration of particle species i, $S_S = d_S f_S(d_L/d_S)$, $S_D = \bar{d}f_D(\rho_H/\rho_L)$, and the functional forms of the size or density ratio dependent functions f_S and f_D are well characterized for size-disperse [16] and density-bidisperse [17] glass-like spherical particles in DEM simulations. Note that the percolation velocity $w_{p,i}$ depends on the local species concentration, $1-c_i$, while the segregation rate w_S in this study is calculated for the entire bed of particles over a window of time in which the local concentration is changing, with the average value in the shear cell over the sampling time window corresponding to about $c_i = 0.55$ for these cases. Aside from this difference, the segregation rate w_S and the percolation velocity $w_{p,i}$ are analogous descriptions of the rate of segregation of species i in a shearing granular flow.

Based on this analogy, we propose a revised expression for the percolation velocity as

$$w_{p,i} = \sqrt{\bar{\rho}g\bar{d}/P\bar{d}}f(R)\dot{\gamma}(1-c_i), \tag{4}$$

where $f(R)$ is $f_S(d_L/d_S)$ for size segregation or $f_D(\rho_H/\rho_L)$ for density segregation, and the average particle diameter $\bar{d}$ is used in the relation for S_S instead of the small particle diameter d_S. Equation 4 can be rewritten as

$$w_{p,i}/\sqrt{g\bar{d}} = If(R)(1-c_i). \tag{5}$$

The linear dependence of $w_{p,i}$ on I in Eq. 5 is consistent with the nearly linear dependence of w_S on I in Fig. 12. Note that as the overburden vanishes for thin free surface flows, which was the case in previous studies [16–18], the bed-induced pressure approaches the limit of a single layer of particles, $\sqrt{\bar{\rho}g\bar{d}/(\bar{\rho}g\bar{d})} = 1$, reducing Eq. 4 back to the form in Eqs. 2 and 3. Further note that the correction term for overburden pressure tends to a reasonable limit ($\sqrt{\bar{\rho}g\bar{d}/P} = 0$) as the gravitational acceleration approaches zero, for which there is no segregation for uniform shear flows [41], or as the pressure becomes large at high overburden, which is the case studied here. Validating this correction factor for $w_{p,i}$ is beyond the scope of this study, but should be considered for future research.

V. DISCUSSION

Through a series of DEM simulations of shearing granular flows, we have quantified the effect of overburden pressure on segregation in equal volume size and density bidisperse flows. The impact of overburden pressure on segregation is only moderately sensitive to particle stiffness, despite the fact that the packing fraction varies substantially with particle stiffness.

While the particle-scale mechanisms through which confining pressure affects segregation are not yet clear, good collapse of the data for the ultimate degree of segregation occurs for both size bidisperse and density bidisperse mixtures as a function of the overburden pressure normalized by the lithostatic pressure of the particle bed, $P/(\rho_B gh)$, under a range of flow conditions (changing P, $\dot{\gamma}$, g, $\bar{\rho}$, and $\bar{d}$). Interestingly, size segregation occurs to a small extent even at large overburden pressures, while density segregation ceases at normalized overburden pressures above a critical pressure, suggesting different underlying mechanisms that drive size segregation and density segregation.

The segregation rate depends on the pressure-shear rate state as characterized by the inertial number I. A power law collapse of segregation rate occurs as a function of I for size bidisperse segregation and I^* for density

segregation under varying flow conditions corresponding to a range of inertial numbers spanning two orders of magnitude. An additional critical pressure cutoff term is necessary for density segregation, because density segregation ceases at a finite normalized overburden. The form of the dependence of the segregation rate on the shear rate and particle size is similar to that for the percolation velocity [16–18] based on the kinetic sieving/squeeze expulsion mechanism proposed by Savage and Lun [2], with the addition of a factor $\sqrt{\bar{\rho}gd/P}$ accounting for the effects of the overburden pressure. In future work, it would be instructive to compare the segregation predicted using this pressure dependence correction with experimental or computational results in more complicated granular flows under confining pressure.

Several questions remain unanswered. The connection between the trace concentration sinking particle cases [14, 15] and the present results should be addressed, which is most easily accomplished by varying the relative concentrations of the two particle species. And, of course, experimental verification of the DEM simulation results would be appropriate, though implementing such an experiment in a well-controlled fashion would likely be challenging. Finally, the mechanism through which segregation is suppressed as the overburden pressure increases is not clear. Beyond showing that void space arguments described in Section III B do not explain the effect, we have also analyzed both pressure and temperature partitioning effects [4, 24, 42], but they also do not explain the observed trends. Despite the remaining questions, the effects of pressure on segregation in granular materials could have significant implications in geophysical flows and dry granular lubrication [5, 8, 11].

ACKNOWLEDGMENTS

Funded by the Procter & Gamble Company and NSF Grant No. CBET-1511450.

Appendix A: Simulation method

Uniform shear flows of granular materials are simulated using a discrete element method (DEM) for deformable spheres [43]. The contact equations are $\mathbf{f_{ij}^n} = \left[k_n\zeta - 2\gamma_n m_{eff}(\mathbf{V}_{ij}\cdot\hat{\mathbf{r}}_{ij})\right]\hat{\mathbf{r}}_{ij}$ for normal contacts and $f_{ij}^t = \min\left\{|k_t\beta - 2\gamma_t m_{eff}(\mathbf{V}_{ij}\times\hat{\mathbf{r}}_{ij})|, |\mu\mathbf{F}_{ij}^n|\right\}\mathrm{sgn}(\beta)\hat{\mathbf{s}}$ for tangential contacts. In the case of static tangential contact, the tangential displacement is given by $\beta(t) = \int_{t_s}^{t} V_{ij}^t dt$ [44], where V_{ij}^t is the instantaneous tangential velocity between contacting particle surfaces, t is the current time, and t_s is the time of initial contact. In the case of sliding tangential contact, the friction coefficient is $\mu = 0.4$. The normal collision parameters are calculated as $k_n = \left[(\pi/t_c)^2 + \gamma_n^2\right]m_{eff}$ and $\gamma_n = -\ln(\varepsilon)/t_c$, and the tangential parameters are calculated as $k_t = 2/7k_n$ and $\gamma_t = 2/7\gamma_n$, where $\varepsilon = 0.8$ is the restitution coefficient, $m_{eff} = m_1m_2/(m_1+m_2)$ is the effective mass per collision, and $1.25\times10^{-4}\,\mathrm{s} \le t_c \le 1\times10^{-3}\,\mathrm{s}$ is the tested range of binary collision time. Note that the particle stiffness k changes with the inverse square of the binary collision time, t_c. Particle-wall collisions are modeled as flat frictional planes using the same contact equations as particle-particle collisions.

Note the addition of a tangential damping term with respect to our previous work [16, 45]. This was added, because in DEM simulations under confining pressure particles have a tendency to oscillate about contact points in static loading, which causes nonphysical enduring kinetic energies in a particle bed that ought to be static, although the nonphysical kinetic energies are several orders of magnitude smaller than the translational kinetic energies of the particles during shear flow. The integration scheme used is the symplectic Euler algorithm, but results from simulations using either the symplectic Euler or the modified velocity Verlet algorithm [46] display no significant differences. The same symplectic Euler algorithm is used to calculate the vertical position of the top wall, according to the balance between the wall weight and contact forces with the top layer of particles (as discussed in Section II). For numerical stability, the integration timestep is $\Delta t = t_c/40$ [16].

[1] J. A. Drahun and J. Bridgwater, Powder Tech. **36**, 39 (1983).
[2] S. B. Savage and C. K. K. Lun, J. Fluid Mech. **189**, 311 (1988).
[3] J. M. Ottino and D. V. Khakhar, Annu. Rev. Fluid Mech. **32**, 55 (2000).
[4] J. M. N. T. Gray and A. R. Thornton, Proc. R. Soc. A **461**, 1447 (2005).
[5] A. Damsgaard, D. L. Egholm, J. A. Piotrowski, S. Tulaczyk, N. K. Larsen, and K. Tylmann, J. Geophys. Res.: Earth Surface **118**, 2230 (2013).
[6] B. Remy, B. J. Glasser, and J. G. Khinast, AIChE journal **56**, 336 (2010).
[7] H. Heshmat, Lubr. Eng. **48**, 373 (1992).
[8] W. G. Sawyer and J. A. Tichy, J. Tribology **123**, 777 (2001).
[9] E. Y. A. Wornyoh, V. K. Jasti, and C. F. Higgs, J. Tribology **129**, 438 (2007).
[10] E. Linares-Guerrero, C. Goujon, and R. Zenit, J. Fluid Mech. **593**, 475 (2007).
[11] B. P. Kokelaar, R. L. Graham, J. M. N. T. Gray, and J. W. Vallance, Earth and Planetary Sci. Lett. **385**, 172 (2014).
[12] K. M. Hill and Y. Fan, Phys. Rev. Lett. **101**, 088001 (2008).
[13] L. A. Golick and K. E. Daniels, Phys. Rev. E **80**, 042301

(2009).
[14] N. Khola and C. Wassgren, Powder Tech. **288**, 441 (2016).
[15] S. Liu and J. J. McCarthy, Phys. Rev. E **96**, 020901 (2017).
[16] C. P. Schlick, Y. Fan, A. B. Isner, P. B. Umbanhowar, J. M. Ottino, and R. M. Lueptow, AIChE J. **61**, 1524 (2015).
[17] H. Xiao, P. B. Umbanhowar, J. M. Ottino, and R. M. Lueptow, Proc. R. Soc. A **472**, 20150856 (2016).
[18] Y. Fan, C. P. Schlick, P. B. Umbanhowar, J. M. Ottino, and R. M. Lueptow, J. Fluid Mech. **741**, 252 (2014).
[19] E. Lerner, G. Düring, and M. Wyart, Proc. Nat. Acad. Sci. USA **109**, 4798 (2012).
[20] The velocity control parameter varies with overburden and depth, over the range $0.0312\,\mathrm{kg/s} \leq A \leq 1.65\,\mathrm{kg/s}$.
[21] V. N. Dolgunin and A. A. Ukolov, Powder Tech. **83**, 95 (1995).
[22] J. M. N. T. Gray and V. A. Chugunov, J. Fluid Mech. **569**, 365 (2006).
[23] L. B. H. May, L. A. Golick, K. C. Phillips, M. Shearer, and K. E. Daniels, Phys. Rev. E **81**, 051301 (2010).
[24] K. M. Hill and D. S. Tan, J. Fluid Mech. **756**, 54 (2014).
[25] P. Gajjar and J. M. N. T. Gray, J. Fluid Mech. **757**, 297 (2014).
[26] K. van der Vaart, P. Gajjar, G. Epely-Chauvin, N. Andreini, J. M. N. T. Gray, and C. Ancey, Phys. Rev. Lett. **114**, 238001 (2015).
[27] R. P. Jones, A. B. Isner, H. Xiao, J. M. Ottino, P. B. Umbanhowar, and R. M. Lueptow, In review.
[28] L. Jing, C. Y. Kwok, and Y. F. Leung, Phys. Rev. Lett. **118**, 118001 (2017).
[29] L. Bridgwater, W. S. Foo, and D. J. Stephens, Powder Tech. **41**, 147 (1985).
[30] D. V. Khakhar, J. J. McCarthy, and J. M. Ottino, Phys. Fluids **9**, 3600 (1997).
[31] A. Tripathi and D. V. Khakhar, J. Fluid Mech. **717**, 643 (2013).
[32] J. N. Roux and G. Combe, Comptes Rendus Physique **3**, 131 (2002).
[33] R. K. McGeary, J. Amer. Ceramic Soc. **44**, 513 (1961).
[34] J. Bridgwater, Powder Tech. **25**, 129 (1980).
[35] B. Utter and R. P. Behringer, Phys. Rev. E **69**, 031308 (2004).
[36] Y. Fan, P. B. Umbanhowar, J. M. Ottino, and R. M. Lueptow, Phys. Rev. Lett. **115**, 088001 (2015).
[37] C. P. Schlick, A. B. Isner, P. B. Umbanhowar, R. M. Lueptow, and J. M. Ottino, Industrial & Engineering Chemistry Research **54**, 10465 (2015).
[38] G. D. R. MiDi, Eur. Phys. J. E **14**, 341 (2004).
[39] P. Jop, Y. Forterre, and O. Pouliquen, Nature **441**, 727 (2006).
[40] Note that three data points from Figure 11(b) do not appear in Figure 12(b), since the values for w_S are 0. Also note that two data points in Figure 12(b) do not appear in Figure 12(c), since I^* is undefined when $P > P_{crit}$. We assume that segregation rate $w_S = 0$ at $P > P_{crit}$ for density bidisperse cases.
[41] Y. Fan and K. M. Hill, New J. Phys. **13**, 095009 (2011).
[42] K. M. Hill and Y. Fan, KONA Powder and Particle Journal **33**, 150 (2016).
[43] P. A. Cundall and O. D. Strack, Géotechnique **29**, 47 (1979).
[44] J. Shäfer, D. Dippel, and D. E. Wolf, J. Phys. I **6**, 5 (1996).
[45] Y. Fan, P. B. Umbanhowar, J. M. Ottino, and R. M. Lueptow, Proc. R. Soc. A **469**, 20130235 (2013).
[46] G. H. Ristow, *Pattern formation in granular materials*, 164 (Springer Science & Business Media, 2000).